Off-axis interferometric phase microscopy with tripled imaging area

Irena Frenklach, Pinhas Girshovitz, and Natan T. Shaked*

Department of Biomedical Engineering, Faculty of Engineering, Tel-Aviv University, Tel-Aviv 69978, Israel
*Corresponding author: nshaked@tau.ac.il

We present an interferometric approach, referred to as interferometry with tripled-imaging area (ITIA), for tripling the quantitative information that can be collected in a single camera exposure while using off-axis interferometric imaging. ITIA enables optical multiplexing of three off-axis interferograms onto a single camera sensor without changing the imaging-system characteristics, such as magnification and spatial resolution, or losing temporal resolution (no scanning is involved). This approach is useful for many applications in which interferometric and holographic imaging are used. Our experimental demonstrations include quantitative phase microscopy of a transparent U.S. Air Force 1951 test target, thin diatom shells, and live human cancer cells. © 2014 Optical Society of America

OCIS codes: (120.3180) Interferometry; (090.1995) Digital holography; (090.4220) Multiplex holography; (120.4640) Optical instruments; (110.3175) Interferometric imaging.
http://dx.doi.org/10.1364/OL.39.001525

Interferometric phase microscopy (IPM) is a quantitative method for capturing an interference pattern between the light interacting with a microscopic sample and a reference beam, and processing it into the sample complex wave front. This wave front contains both the amplitude modulation and the quantitative phase delays induced by the sample. It has been shown that IPM can be used for a wide range of purposes, such as biological cell investigations [1–6] and nondestructive tests [7–12].

In on-axis interferometry, where there is no angle between the reference and the sample beams creating the interference, typically three or four interferograms are required in order to extract the complex wave front of the sample [13], which might be limiting when acquiring dynamic objects. In off-axis interferometry, on the other hand, due to a small angle between the sample and the reference beams, it is possible to reconstruct the complex wavefront from a single interferogram, and therefore the dynamic sample recording is limited only by the full frame rate of the digital camera.

While being an invaluable tool for biological and medical research, most IPM setups are bulky and hard to align and operate. Therefore, they are currently not widely used in biology and medicine. Various portable and easy-to-align modules have been presented lately [14–17], allowing inexperienced users to enjoy the benefits of IPM.

Frequently, in spite of using scan-free off-axis interferometry, a single field of view (FOV) is not enough for capturing the entire sample of interest. This might happen because the interferometric image is wider than the camera sensor or because the sample is dynamic and might leave the FOV during its acquisition. Of course, it is possible to scan the sample in order to record a wider FOV. However, for highly dynamic samples, it is inapplicable since the sample might move by the time the scan is over. Another simple solution is to decrease the imaging system magnification, but this is not always possible due to potential loss of small details in the image [18].

Another approach for increasing the recorded FOV is multiplexing several FOVs onto the same camera sensor. This approach has been implemented in both interferometric [19] and noninterferometric [20,21] imaging setups. However, so far, this multiplexing has been done in the time domain, thus, again, reducing dynamic imaging capabilities.

Lately, we have developed a new approach for extending the recorded FOV in off-axis interferometry without loss in the imaging parameters, such as magnification or spatial resolution and without reducing the temporal resolution (since only a single exposure is needed). This approach, called interferometry with doubled-imaging area (IDIA) [18], is able to optically compress two off-axis interferometric FOVs taken from different areas on the sample onto a single camera sensor. This is done by optically multiplexing two orthogonally rotated off-axis interferograms on the same camera FOV. Depending on the optical alignment, these FOVs can be continuous or located in far places on the sample. We implemented this technique using a compact interferometric module located at the output of the imaging system, just in front of the digital camera.

In [18], we have demonstrated the advantages of this technique for imaging stationary and dynamic biological samples with fine details, as well as for dynamic profiling during a lithography process. We have also shown that this technique is able to double the off-axis interference area, even if it is limited due to using a low-coherence illumination. Using a high-resolution test target, we have shown in [18] that the interferometric multiplexing does not damage the spatial resolution, and thus this multiplexing is not similar to simply demagnifying the image to squeeze it into a single camera sensor, which might damage the spatial resolution.

In this Letter, we extend the IDIA principle and present a new technique in which we are able to multiplex three off-axis interferograms onto a single camera sensor without loss in the imaging parameters or in the temporal resolution. We refer to this technique as interferometry with tripled-imaging area (ITIA). Here as well, the suggested

system is based on a compact interferometric module located at the output of the imaging system.

Figure 1 presents a possible optical setup for demonstrating the ITIA principle. In this setup, we use an inverted transmission microscope illuminated by a HeNe laser. This microscope contains a microscope objective (MO) and a tube lens (L_0). The sample is projected onto the image plane at the output of the microscope, where the ITIA module is placed.

The magnified image at the microscope output is Fourier transformed by lens L_1 and split by beam-splitter BS_1 into the reference and preliminary sample beams. The final reference beam is then created by spatially filtering out the sample modulation using pinhole PH [14,15]. The preliminary sample beam at the exit of BS_1 is split into three sample beams by beam-splitters PBS and BS_2. At each beam-splitter exit, there is a retro-reflector, which reflects the beam back in a different
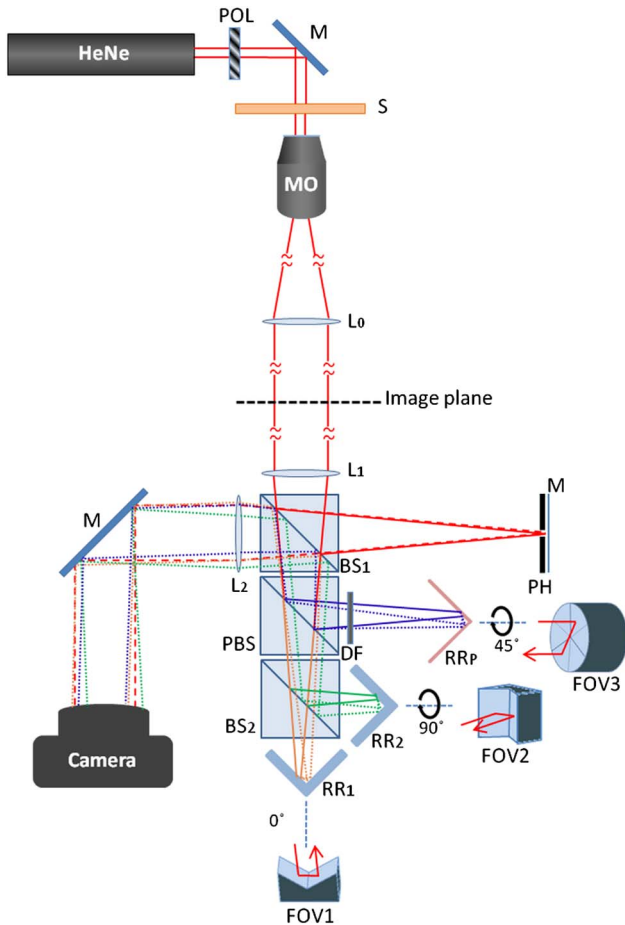
Fig. 1. ITIA module, connected at the output of a simple inverted microscope. The blue beams represent S-polarized light, while the orange and the green beams represent P-polarized light. HeNe, Helium–Neon laser (wavelength of 632.8 nm); S, sample; MO, microscope objective (40×; 0.66 NA, infinity corrected); L_0, L_1, L_2, lenses (focal lengths: 16, 16, and 15 cm); POL, 45° polarizer; BS_1, BS_2, beam splitters; PBS, polarizing beam splitter (PBS251, Thorlabs); DF, density filter; M, mirror; PH, 30 μm pinhole; RR_1, RR_2, retro-reflectors made out of two mirrors connected at a right angle; RR_p, retro-reflector made out of a total internal reflection prism (PS975M-A, Thorlabs). Camera, monochrome digital camera (DCC1545M, Thorlabs). Camera sensor size: 5.32 mm × 6.65 mm.

angle, while shifting the Fourier-domain origin transversally [18]. The beams reflected from RR_1 and RR_2 are orthogonally rotated compared to each other, and the beam reflected from RR_p is rotated at 45° compared to the beam from each of the other two retro-reflectors. Each of the three sample beams is then combined with the final reference beam using the beam-splitters, and inverse Fourier transformed onto the camera by lens L_2, which is positioned in $4f$ lens configuration with lens L_1. Because of the Fourier shift induced by the retro-reflectors, we obtain three off-axis interferences on the camera, with fringes rotated at 45° compared to each other. Each retro-reflector also rotates the sample image. Therefore, if the projected sample image is larger than the camera sensor size, we actually project three sample FOVs onto the same camera sensor. If the sample is mostly transparent (such as live cells *in vitro*), we can image all sample FOVs at once.

To avoid unwanted interferences between the sample beams, we use polarization effects. First, we illuminate the sample by 45°-polarized light (using linear polarizer POL in front of the laser). Therefore, the reference beam has both P and S polarization states. After splitting the beam in the polarizing beam-splitter PBS, S polarization is reflected and P polarization is transmitted. Therefore, the two FOVs reflected by RR_1 and RR_2 are P-polarized, and after they interfere with the P-polarized part of the reference beam, two orthogonal off-axis interferograms are created on the camera. RR_1 and RR_2 are built by connecting two mirrors at 90°. RR_P, on the other hand, is a total-internal-reflection prism, turning the linearly polarized light into elliptically polarized light [22], which enables us to adjust the retro-reflector so that the S-polarization will not be blocked by PBS. Using right-angle mirror retro-reflector instead of RR_P would rotate the light polarization upon reflection, and the light would be blocked by PBS.

Figure 2 presents ITIA for transparent polymer microspheres. As shown in Fig. 2(a), four interferences are recorded by the camera at once—three interferences between the three sample beams and the reference beam, and another one between the two P-polarized sample beams. This multiplexed interferogram is described as

$$|E_{s1}^{(P)} + E_{s2}^{(P)} + E_{s3}^{(S)} + E_r^{(P+S)}|^2 = |E_{s1}^{(P)}|^2 + |E_{s2}^{(P)}|^2 + |E_{s3}^{(S)}|^2$$
$$+ |E_r^{(P+S)}|^2 + E_{s1}^{(P)} E_{s2}^{*(P)} + E_{s1}^{*(P)} E_{s2}^{(P)} + E_{s1}^{(P)} E_r^{*(P+S)}$$
$$+ E_{s1}^{*(P)} E_r^{(P+S)} + E_{s2}^{(P)} E_r^{*(P+S)} + E_{s2}^{*(P)} E_r^{(P+S)}$$
$$+ E_{s3}^{(S)} E_r^{*(P+S)} + E_{s3}^{*(S)} E_r^{(P+S)}, \qquad (1)$$

where $E_{s1}^{(P)}$ and $E_{s2}^{(P)}$ are the P-polarized sample beams (of FOV1 and FOV2, respectively), $E_{s3}^{(S)}$ is the S-polarized sample beam (of FOV3), and $E_r^{(P+S)} = E_r^{(P)} + E_r^{(S)}$ is the reference beam. The first four elements on the right side of Eq. (1) represent the wave intensities, and in the Fourier domain [see Fig. 2(b)] will be translated to auto-correlations located at the center. The other eight elements create the off-axis interferences, which are rotated at 45° compared to each other. In the Fourier domain, the resulting cross-correlations will be shifted
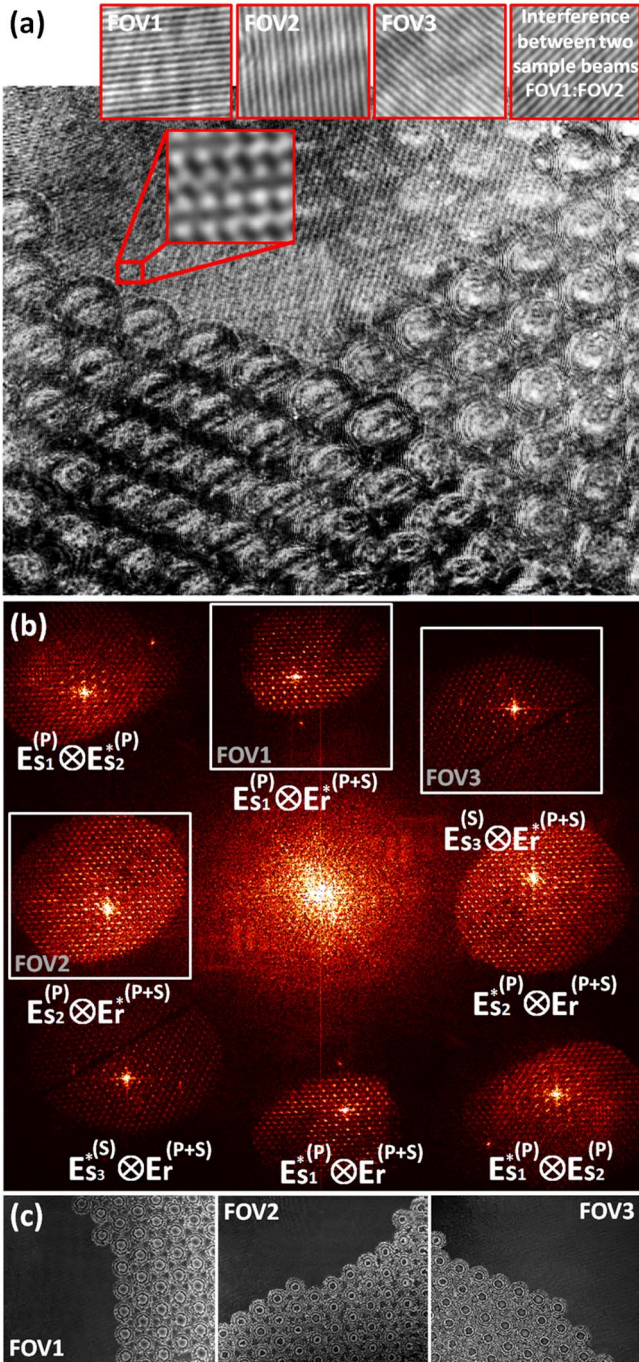
Fig. 2.   ITIA for imaging 15 μm clear polymer microspheres. (a) The optically multiplexed interferogram. In the upper red boxes: a magnified region from this multiplexed interferogram, and the off-axis interference patterns encoded into this interferogram. (b) Fourier (spatial-frequency) domain. $\otimes$ between **E**s represents two-dimensional spatial convolution, where **E**s represent the spatial Fourier transforms of the coinciding Es. (c) Reconstructed wrapped phase images of the three FOVs.

to different locations far from the origin [see Fig. 2(b)]. Therefore, we can reconstruct the phase profiles of the three FOVs [see Fig. 2(c)]. Note that $E_{s3}^{(S)}$ does not interfere with $E_{s1}^{(P)}$ or $E_{s2}^{(P)}$ due to their orthogonal polarizations.

The digital reconstruction process [15] includes spatial filtering, applied digitally three times, once for

each cross-correlation between a sample beam and the reference beam. The first reconstruction is applied when filtering $E_{s1}^{(P)}E_r^{*(P+S)}$, the second one is when filtering $E_{s2}^{(P)}E_r^{*(P+S)}$, and the third one is when filtering $E_{s3}^{(S)}E_r^{*(P+S)}$. Each of the filtered regions is indicated in Fig. 2(b) by a white box.

The ability to multiplex several interferograms into one is due to a property previously considered as a disadvantage of the off-axis inteferometric geometry, according to which the Fourier domain should be at least eight times broader than the highest spatial frequency recorded, typically related to the optical resolution limit [18]. Under the assumption that the maximum spatial frequencies in the x and the y directions are equal, this off-axis encoding creates an empty space for additional cross-correlation elements in other directions around the Fourier-domain origin, to which we compress additional data without overlaps with the other elements.

We then created an optically transparent 1951 U.S. Air Force test target on a glass plate using a photolithography process of UV-cured adhesive. Figure 3 shows the full test target containing groups 6 and 7, and the quantitative phase profiles of the three FOVs imaged simultaneously using the ITIA technique. Since the magnified image size of the test target is 10.96 mm × 10.96 mm, which is larger than our camera sensor size (5.32 mm × 6.65 mm), these three FOVs could not be recorded at once without using ITIA.

Next, we used ITIA to quantitatively image microscopic diatom shells (Microlife Services, England). Figure 4(a) presents the multiplexed off-axis interferogram, in which several overlapping diatoms can be seen. Figures 4(b)–4(d) present the three quantitative phase profiles reconstructed from this multiplexed interferogram. It can be seen that the shells presented in the multiplexed interferogram are actually three separable
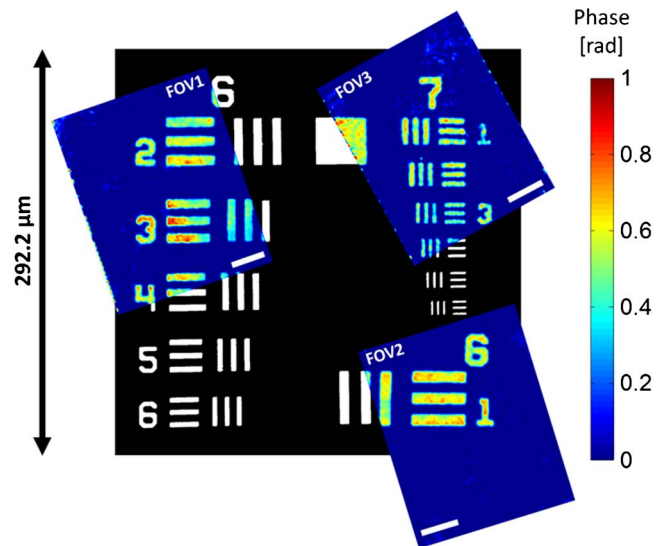
Fig. 3.   ITIA for quantitative phase imaging of a 1951 U.S. Air Force phase target. In black and white—the full target, which is larger than the camera sensor under the magnification used. Three simultaneously acquired quantitative unwrapped phase images are shown on top. The white scale bars indicate 27.62 μm.
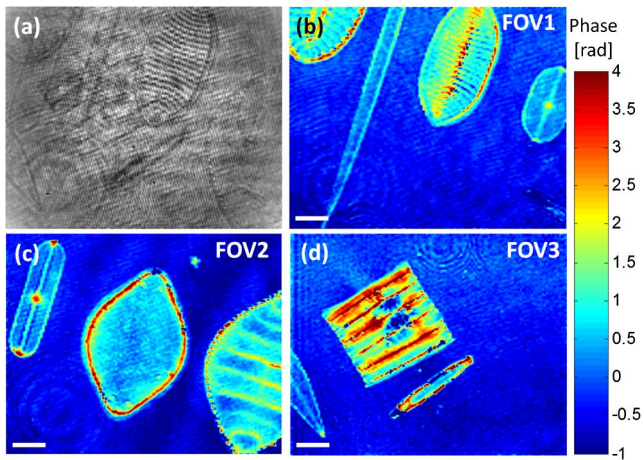
Fig. 4.   ITIA for quantitative phase imaging of microscopic diatom shells. (a) Multiplexed off-axis interferogram containing three FOVs. (b)–(d) Reconstructed quantitative unwrapped phase profiles of the three FOVs. The white scale bars indicate 20 μm.
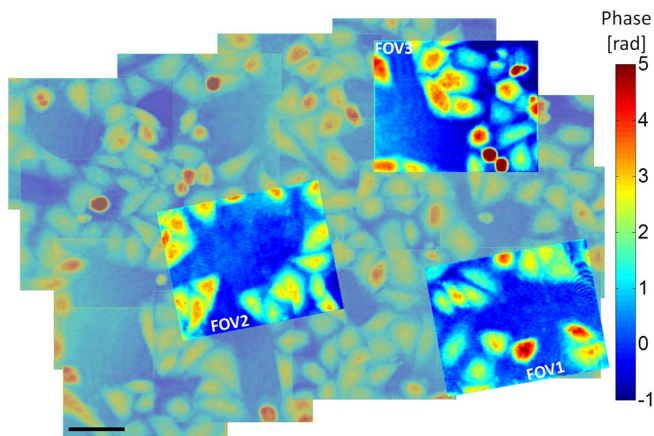
Fig. 5.   ITIA for quantitative phase imaging of HeLa cells. In muted colors—the scanned FOV (larger than the camera FOV). Three quantitative unwrapped phase images reconstructed from a single multiplexed interferogram acquired simultaneously, without any scanning. The black scale bar indicates 50 μm.

FOVs, acquired simultaneously using a single camera exposure.

Our last demonstration includes quantitative phase imaging of live HeLa cells (human cervical cancer, purchased from ATCC). As presented in Fig. 5, we first scanned a broad area of 4×4 frames (presented as muted-color background). Next, we used ITIA to record three FOVs from the sample simultaneously, while enabling quantitatitve imaging of larger cell population at once.

In this Letter, we presented the ITIA technique for tripling the off-axis interferometric FOV acquired in a single camera exposure. We used the fact that orthogonal polarizations do not interfere in order to optimize the Fourier-domain usage. The three simultaneously obtained FOVs do not overlap in the Fourier domain, so that

all of them can be acquired at once. The fact that we used highly coherent source enabled us to obtain interference on the entire camera sensor, thus tripling the entire camera FOV, while sharing the camera dynamic range. As demonstrated for IDIA [18], the FOVs can be adjacent, so that we could reconstruct a single continuous FOV that is three times larger than the original FOV. We demonstrated the ITIA technique by quantitative phase imaging of a phase test target and biological samples, where objects (e.g., cells) located in the extended FOV can be investigated simultaneously.

References

1. P. Girshovitz and N. T. Shaked, Biomed. Opt. Express **3**, 1757 (2012).
2. M. Mir, Z. Wang, Z. Shen, M. Bednarz, R. Bashir, I. Golding, S. G. Prasanth, and G. Popescu, P. Natl. Acad. Sci. USA **108**, 13124 (2011).
3. Y. Bishitz, H. Gabai, P. Girshovitz, and N. T. Shaked, J. Biophoton. **7**, 1 (2013).
4. V. P. Tychinsky, A. V. Kretushev, I. V. Klemyashov, T. V. Vyshenskaya, N. A. Filippova, N. T. Raikhlin, and A. A. Shtil, J. Biomed. Opt. **13**, 064032 (2008).
5. G. Popescu, Y. Park, W. Choi, R. R. Dasari, M. S. Feld, and K. Badizadegan, Blood Cell Mol. Dis. **41**, 10 (2008).
6. N. T. Shaked, L. L. Satterwhite, M. J. Telen, G. A. Truskey, and A. Wax, J. Biomed. Opt. **16**, 030506 (2011).
7. A. Finizio, P. Ferraro, S. De Nicola, M. Iodice, S. Grilli, and G. Coppola, Meas. Sci. Technol. **15**, 529 (2004).
8. F. Charrière, J. Kühn, T. Colomb, F. Montfort, E. Cuche, Y. Emery, K. Weible, P. Marquet, and C. Depeursinge, Appl. Opt. **45**, 829 (2006).
9. S. De Nicola, P. Ferraro, A. Finizio, S. Grilli, G. Coppola, M. Iodice, P. De Natale, and M. Chiarini, Meas. Sci. Technol. **15**, 961 (2004).
10. H. Gabai, M. Baranes-Zeevi, M. Zilberman, and N. T. Shaked, Opt. Lett. **38**, 3017 (2013).
11. G. Coppola, V. Striano, P. Ferraro, S. De Nicola, A. Finizio, G. Pierattini, and P. Maccagnani, J. Microelectromech. Syst. **16**, 659 (2007).
12. L. Xu, X. Peng, J. Miao, and A. K. Asundi, Appl. Opt. **40**, 5046 (2001).
13. J. Garcia-Sucerquia, W. Xu, S. K. Jericho, P. Klages, M. H. Jericho, and H. J. Kreuzer, Appl. Opt. **45**, 836 (2006).
14. N. T. Shaked, Opt. Lett. **37**, 2016 (2012).
15. P. Girshovitz and N. T. Shaked, Opt. Express **21**, 5701 (2013).
16. B. Kemper, A. Vollmer, C. E. Rommel, J. Schnekenburger, and G. Von Bally, J. Biomed. Opt. **16**, 026014 (2011).
17. Z. Wang, L. Millet, M. Mir, H. Ding, S. Unarunotai, J. Rogers, M. U. Gillette, and G. Popescu, Opt. Express **19**, 1016 (2011).
18. P. Girshovitz and N. T. Shaked, "Doubling the field of view in off-axis low-coherence interferometric imaging," Light: Sci. Appl. **3**, E152 (2014).
19. M. Paturzo, P. Memmolo, A. Tulino, A. Finizio, and P. Ferraro, Opt. Express **17**, 8709 (2009).
20. S. Uttam, N. A. Goodman, M. A. Neifeld, C. Kim, R. John, J. Kim, and D. Brady, Opt. Express **17**, 1691 (2009).
21. V. Treeaporn, A. Ashok, and M. A. Neifeld, Opt. Express **18**, 22432 (2010).
22. J. Liu and R. M. Azzam, Appl. Opt. **36**, 1553 (1997).